Advances in Aircraft and Spacecraft Science, *Vol. 9, No. 5 (2022) 479-491*
https://doi.org/10.12989/aas.2022.9.5.479

Q1D modeling of hydrodynamic instabilities in solid rocket motors

M. Grossi*, D. Bianchi[a] and B. Favini[b]

Department of Mechanical and Aerospace Engineering, Sapienza University of Rome, Via Eudossiana 18, 00184, Italy

(Received February 25, 2022, Revised September 8, 2022, Accepted September 12, 2022)

Abstract. This work concerns the investigation of a Q1D methodology employed to study pressure oscillations in solid rocket motors driven by hydrodynamic instabilities. A laboratory-scale solid motor designed to develop vortex-shedding phenomena is analyzed for the whole firing time. The comparison between numerical results and experimental data shows good agreement regarding pressure oscillations signature, especially in the flute-mode behavior, the typical oscillations frequency trend present in any motor liable to hydrodynamic instabilities. Such result ensures the model capability to cope with this particular kind of pressure oscillations source, allowing the investigation of the phenomenon with a lighter and cost savings methodology than CFD simulations.

Keywords: Q1D model; solid rocket motors; vortex-shedding

1. Introduction

The operational time of a solid rocket motor (SRM) may be divided into three separated phases: ignition transient, quasi-steady state, and tail-off. Depending on the motor system design, each phase may potentially present an unstable behavior, characterized by different properties. During the quasi-steady state, pressure oscillations (PO), featuring a low amplitude sinusoidal shape, are driven by a feedback loop phenomenon, arising from the coupling among the internal combustion and flow processes with the motor natural acoustic modes (Culick and Kuentzmann 2006). Nowadays, such an issue still represents an open problem for motors currently flying as the P80 (Laureti *et al.* 2018) and the P120C (Larrieu *et al.* 2018), the large boosters employed in the present European scenario. As a matter of fact, modern solid motors are required to be ever more performing and safe, two requirements which can be accomplished ensuring a low level of PO during the operative time. For such reasons, a proper characterization of the motor unsteady behavior represents a mandatory task to achieve during the motor design process.

In the state of the art concerning SRMs unsteady behavior, two major PO sources are currently addressed (Casalis *et al.* 2011, Fabignon *et al.* 2016, Larrieu *et al.* 2018, Orlandi *et al.* 2019): hydrodynamic instabilities, related to vortex-shedding phenomena, and thermoacoustic instability

*Corresponding author, Research Fellow, E-mail: marco.grossi@uniroma1.it
[a]Associate Professor, E-mail: daniele.bianchi@uniroma1.it
[b]Associate Professor, E-mail: bernardo.favini@uniroma1.it

http://www.techno-press.org/?journal=aas&subpage=7 ISSN: 2287-528X (Print), 2287-5271 (Online)

due to the aluminum distributed combustion. Contrary to the quite recent assessment of aluminum combustion as a PO source (Gallier and Godfroy 2009), the periodic shedding of vortices caused by obstructions and its consequent effect on the acoustic field was firstly suggested by Flandro and Jacobs (1973), paving the way to the investigation of this kind of instability in the subsequent years. Since then, the aeroacoustic coupling occurring in SRMs has been definitely assessed via experimental test campaigns (Dunlap *et al.* 1990, Mastrangelo *et al.* 2013, Larrieu *et al.* 2015), analytical and semi-empirical approaches (Rossiter 1964, Chedevergne *et al.* 2006, Bouyges *et al.* 2017, Majdalani *et al.* 2021) and CFD methods (Lupoglazoff and Vuillot 1996, Telara *et al.* 2006, Ballereau *et al.* 2011, Yang *et al.* 2018).

The onset of PO due to hydrodynamic instabilities is related to the generation, transport, and deformation of vortices within the combustion chamber. The fundamental steps of the basic acoustic feedback model may be summed up as Dotson *et al.* (1997): 1) a shear layer is generated at an upstream point and rolls up into a vortex as it travels downstream; 2) vortex deformation due to the flowfield structure generates an acoustic pulse which travels back upstream; 3) the acoustic pulse reaches the shear-layer initiation point and perturbs the shear layer to contribute to a subsequent vortex. As a consequence, if the vortex-shedding frequency is close to an acoustic mode of the chamber, then an aeroacoustic coupling is established, prompting the onset of self-sustained flow oscillations.

Notwithstanding the great advancement in CFD computations possibility, efficient 1D models would be valuable engineering tools in the design process of large SRMs regarding hydrodynamic instabilities risk assessment. These approaches offer huge savings in terms of computing power and time compared to complex multidimensional numerical simulations and, at the same time, can represent the physical phenomenology involved in the vortex-shedding feedback loop once physics-reliant models, more challenging to develop and handle with regard to the ones necessary in CFD simulations, are employed. In this spirit, several attempts to define analytical and low-order models to investigate the vortex-sound production in SRMs nozzle have been reported in the scientific literature (Anthoine *et al.* 2002, Hirschberg *et al.* 2018). A fully Q1D description of the aeroacoustic coupling occurring in SRMs is provided by the Aerodynamically Generated Acoustic Resonance (AGAR) model, in development for the past decade (Ferretti 2011, Laureti and Favini 2019, Grossi *et al.* 2019). In the AGAR model, vortices generation and dynamics are addressed via a specific methodology that implies the resolution of the vorticity equation in a Q1D framework. In particular, vortices are generated following a criterion based on the flowfield evolution and convected towards the nozzle where the flow is excited by ad-hoc source terms.

In the present work, the AGAR model is presented and applied to a simple test case, the ONERA C1xb (Dupays *et al.* 1996), known to be prone to hydrodynamic instabilities due to vortex-shedding. Comparisons with results concerning the semi-empirical Rossiter approach (Rossiter 1964) are reported, together with a qualitative confrontation with CFD data presented in literature, in order to corroborate the Q1D methodology employed in this work.

2. Aerocoustic feedback loop in SRMs

The aeroacoustic feedback loop responsible for the onset of PO in SRMs follows the same physical steps reported in the introductory section, however, some peculiarities typical of SRMs are to be mentioned. In a solid rocket chamber, vortex-shedding may occur through three different mechanisms (Fabignon *et al.* 2003, Culick and Kuentzmann 2006): Obstacle Vortex-Shedding

(OVS), due to the presence of obstacles to the flow motion along the grain wall as inhibitors or slots; Angular Vortex-Shedding (AVS), caused by sharp discontinuities in the chamber geometry; Parietal Vortex-Shedding (PVS), present within motors characterized by marked slenderness able to trigger the Taylor-Culick flow (Taylor 1956, Culick 1966) intrinsic instability. It is worth noting that such distinction is less clear when it comes to complex solid propellant geometries like aft-finocyl designs. In SRMs, the acoustic excitation is usually provided close to the nozzle where the rapid flow acceleration strongly strains the vortical structures. Finally, laminar-turbulent flow transition is thought to play a key role, breaking apart the vortices coherent structures and, consequently, the feedback loop (Fabignon *et al.* 2016).

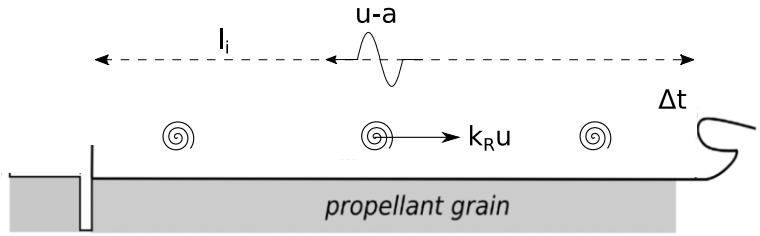

Fig. 1 Rossiter feedback loop model within a SRM

The aforementioned description can be expressed mathematically thanks to the model developed by Rossiter (1964). Such approach is of paramount relevance since it has been widely applied, with excellent results, in unstable SRMs as the Titan IV SRMU (Dotson *et al.* 1997) and the Peacekeeper (Dotson *et al.* 2001). Referring to the schematic representation reported in Fig. 1, the vortex-shedding frequencies of the Rossiter model, valid for low Mach number flowfields, are so defined

$$f_{vs} = \frac{u}{l_i}\frac{m-\alpha}{M+1/k_R} \tag{1}$$

in which l_i is the distance between the shear-layer initiation and sound-production points, u is the free-stream velocity, M is the Mach number, m is the number of vortices lying in l_i distance, k_R is the ratio of the velocity at which the vortices are convected to the free-stream velocity, α a small parameter to account for a time delay, Δt, between vortex deformation and sound production. Note that for SRMs, α and M assume a negligible role, therefore f_{vs} is primarily controlled by the other contributions. A detailed review of such parameters is reported in the work of Dotson *et al.* (1997) that points out an upper limit for the number of vortices and, as a consequence, for the lock-in frequencies. Looking at Eq.1, two important considerations may be drawn. In SRMs, chamber geometry and flow dynamics, respectively expressed by l_i and u, change over time due to the propellant combustion, so vortex shedding frequencies vary as time runs forward. On the other hand, given a certain time instant, there are several frequencies at which the motor can be unstable depending on the number of vortices contemporary present in the chamber. These characteristics are at the base of the flute-mode behavior, the typical time trend shown by the oscillations frequency in motors affected by hydrodynamic instabilities (Dotson *et al.* 1997, Hijlkema *et al.* 2011). Assuming that in a certain time instant the aeroacoustic lock-in occurs, the vortex-shedding frequency matches the acoustic one and the system is characterized by a certain number of

vortices. Then, f_{vs} moves away from the acoustic frequency due to the evolution of the chamber geometry so that when the gap is too wide, a vortex-shedding frequency jump occurs because of the presence of an extra vortex within the chamber. Such discontinuous behavior ensures the development of a different resonant configuration, which allows to recover the acoustic frequency.

3. Q1D modeling

AGAR is a Q1D model developed to address aeroacoustic phenomena in SRMs. Its formulation derives from an in-house flowfield solver based on the single-phase unsteady Q1D Eulerian set of equations enriched with a model for geometry evolution due to the propellant combustion (Cavallini 2009). Vortex-shedding phenomena may be analyzed via a Q1D approach once the aforementioned system of equations is coupled with a further expression that describes the vorticity dynamics within the motor chamber. The latter is formally obtained from the multi-dimensional vorticity equation introducing the assumptions of axisymmetric flow (Ferretti 2011). The full set of equations considered in the AGAR model follows

$$\frac{\partial(\rho A_p)}{\partial t} + \frac{\partial(\rho u\, A_p)}{\partial x} = S_{prop}^{(m)} + S_{cav}^{(m)} \tag{2}$$

$$\frac{\partial(\rho u\, A_p)}{\partial t} + \frac{\partial[(\rho u^2 + p)A_p]}{\partial x} - p\frac{\partial A_p}{\partial x} = S_a^{(q)} \tag{3}$$

$$\frac{\partial(\rho e\, A_p)}{\partial t} + \frac{\partial[(\rho e + p)uA_p]}{\partial x} = S_{prop}^{(e)} + S_{cav}^{(e)} + S_a^{(e)} \tag{4}$$

$$\frac{\partial(\omega A_p)}{\partial t} + \frac{\partial(k_u\, u\omega A_p)}{\partial x} = S_\omega \tag{5}$$

Source terms S_{prop} and S_{cav} are originated from, respectively, the propellant grain combustion, evaluated via the De Saint-Venant law, and the cavity modeling to take into account, in a Q1D formulation, mass and energy exchange with submergence zone located close to the nozzle of typical SRMs configurations (Ferretti 2011). The cavity model is based on a set of ordinary differential equations resulting from averaging of mass and energy balance equations over the cavity volume (Cavallini *et al.* 2015).

Focusing on Eq. (5), two closure terms complete the Q1D equation for vorticity dynamics: S_ω and k_u. The first term represents the instantaneous vorticity source enabled on the shedding point, which may be an obstacle or a geometry discontinuity. The S_ω term is modeled accordingly with the work of Clements (1973), which states that, in presence of vortex-shedding phenomena, the vorticity piled up during the time lapse between two consequent vortex releasing, T_ω, is proportional to the square of the local velocity, u_{vs}. In a Q1D framework, the expression is recast as

$$S_\omega = \int_{T_\omega} \alpha_\Gamma \pi R_p u_{vs}^2\, dt \tag{6}$$

The employing of the α_Γ parameter arises from the closure operation performed on the 3D vorticiy equation to obtain the Q1D formula. The α_Γ may also be related to other physical

phenomena aimed at properly addressing vortex circulation within the motor chamber. Matveev and Culick (2003), in their work about AVS stemming from backward cavity step, employ a calibration coefficient to consider that a portion of the shed vorticity diffuses, not entering the forming vortex. Moreover, in the SRMs scenario, the vorticity levels are strongly affected by the heterogeneous combustion process occurring on the grain surface. Vortex generation, i.e., S_ω onset, is imposed following a flowfield-based criterion: each time a velocity maximum is detected at the generation point, a new vortex is introduced in the ω field. This procedure is justified by the physical phenomenology of the aeroacoustic feedback loop in which the instability of the shear layer that triggers the generation of the vortex is affected by the wave dynamic within the chamber (Flatau and VanMoorhem 1990). It is worth pointing out that only when the velocity oscillations frequency is closed to an acoustic mode of the chamber, a feedback loop may actually develop.

The k_u coefficient acts on the vorticity advection velocity. This term arises since the need to correct the vortex transport velocity obtained from the actual evaluation based on AGAR Q1D modeling. Its functional law may be related to the shedding point velocity. In the present work, the k_u definition is evaluated starting from the time evolution of the velocity at the shedding point, as similarly done by Laureti and Favini (2019).

Finally, in agreement with the Lighthill-Powell-Howe vortex-sound theory (Howe 1998), acoustic emissions are provided by the misalignment between acoustic and vortices velocity vectors. In a solid motor chamber, acoustic excitation is usually due to the strong flow modification close to the nozzle exit. In a Q1D model, such excitement may be provided thanks to the proper source term, S_a, which relates sound production to vortex deformation induced, in turn, by the chamber geometry design. The mathematical formulations for these quantities follow

$$S_a^q = \rho u \omega \pi \frac{\partial R_p}{\partial x} A_p \tag{7}$$

$$S_a^e = u\, S_a^q \tag{8}$$

Concerning the numerical scheme employed for solving Eq. (5), every once the generation criterion is fulfilled, a new impulse in the ω field is imposed only in the cell corresponding to the shedding point. The impulse is conceived like a Dirac delta with amplitude established by the S_ω value. From the shedding point, the newborn vortex is convected, solving the pure transport Eq. 5, towards the nozzle exit, undergoing amplitude reduction due to numerical diffusion.

4. C1xb numerical results

In order to show the capability of the Q1D aeroacoustic model to treat hydrodynamic instabilities, hereafter it is reported and discussed the numerical solution obtained applying the AGAR model to an elementary SRM set-up called C1xb (Dupays *et al.* 1996). The C1xb is a lab-scale SRM designed to study pure vortex-shedding phenomena occurring within solid rocket motors chambers. As shown in Fig.2, the motor geometry is characterized by a tubular case 0.7 m long, occupied in the first half by a cylindrical propellant grain presenting a chamfered edge right in the middle of the chamber. Such geometrical configuration is particularly suited to develop hydrodynamic instabilities: as demonstrated by the work of Dunlap and Brown (1981), the aeroacoustic feedback loop for the odd longitudinal modes is maximized if the shedding point corresponds to a velocity antinode, the spatial point in which the wave mode presents the largest

oscillation. During the experimental test campaign carried out with the C1xb, several propellant formulations have been used, however, the firing of interest for this paper regards the results obtained with a non-aluminized propellant in order to deal with a pure one-phase flowfield.

The C1xb geometry may be treated with AGAR code once the model calibration is performed. The shedding point is imposed at the end of the propellant grain, whereas the k_u evolution is investigated via a multidimensional analysis carried out on the motor geometry. Since the very simple design, the flowfield structure is marginally affected over time, i.e., only in terms of mass flowrate values, thus just a fixed geometry, referring to a certain time instant, is simulated to explore the relationship between multidimensional and Q1D fields. Naturally, such an approach

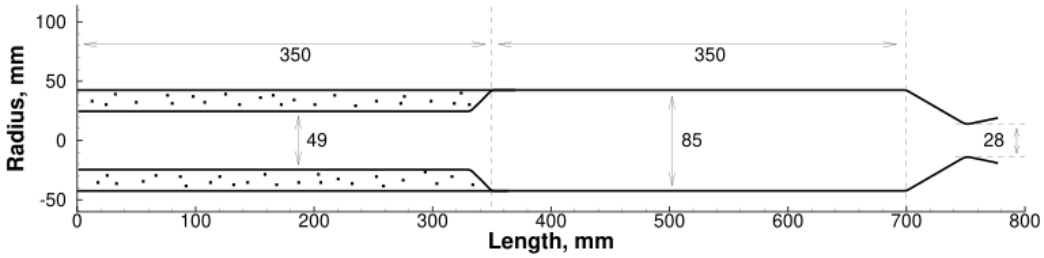

Fig. 2 Schematic diagram of the C1xb setup (dimensions are in *mm*) (Dupays *et al.* 1996)

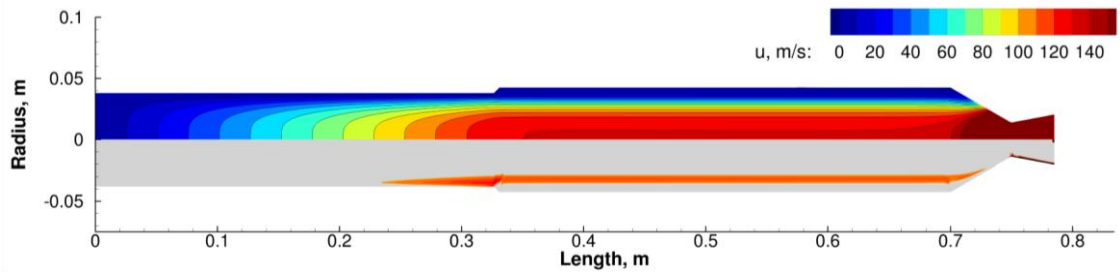

(a) CFD solution. Axial velocity in the upper half, vorticity magnitude in the lower half

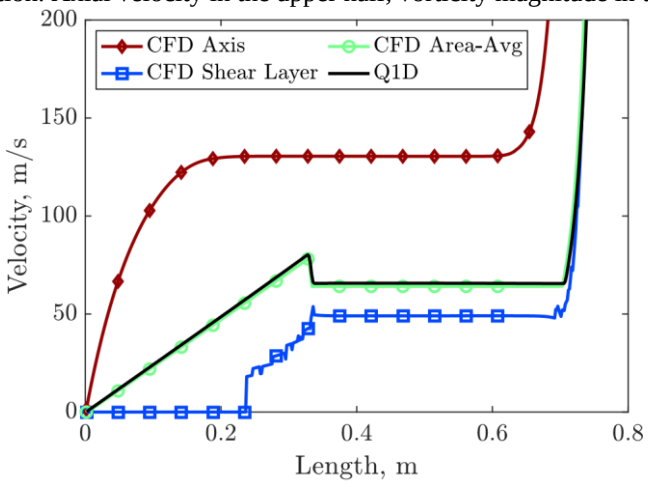

(b) Comparison between CFD and Q1D results

Fig. 3 C1xb flowfield solution

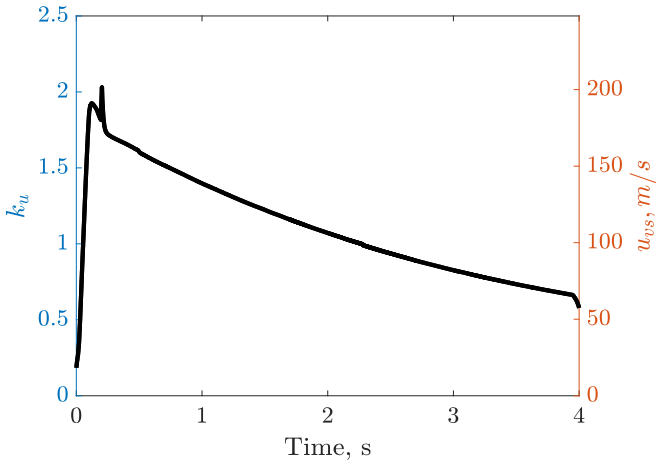

Fig. 4 C1xb k_u trend

can not be considered valid for more complex motor designs for whom several CFD simulations would be required to properly map the overall operational time. It is worth noting that the ultimate goal of such simulations is not to recover the motor PO, but just to gather more information about the mean flow. These requirements allow using light grids with low computational time in order to obtain a stationary field.

To pursue this aim, an axisymmetric simulation is performed solving the unsteady Euler equations via an in-house CFD code used in the field of SRMs (Grossi *et al.* 2020). The results of the aforementioned analysis are presented in Fig. 3. Looking at Fig. 3(a), the steadystate fields of the axial velocity and the vorticity solution are shown. In the first half of the motor, the velocity presents the typical Taylor-Culick profile, whereas right after the end of the propellant grain, the longitudinal velocity is basically unchanged up to the nozzle convergent section. This behavior suggests that the vortex dynamic in the second half of the C1xb is controlled by the velocity profile found at the chamfered edge of the propellant, which, in turn, is a function of the Taylor-Culick flow evolution over time. A corroboration of such statement may be found in Fig. 3(b) that provides a representation of the velocity along the chamber length for both CFD and Q1D computations. As it is possible to see, the velocity estimate of the shear layer is constant beyond the separation point and differs both from the value found on the axis and from that obtained by averaging over the section area. The latter is evaluated through Eq. (9) and presents an excellent agreement with the Q1D velocity trend. For all the reasons mentioned above, the k_u coefficient employed for the C1xb is chosen to follow the time trend of the Q1D velocity at the shedding point, shown in Fig. 4, which represents the area-average of the Taylor-Culick velocity profile, as witnessed in Fig. 3. A parameter obtained comparing the shear-layer velocity of the CFD solution with the Q1D velocity field within the aft-end of the motor is applied to scale the k_u values.

$$u_{avg} = \frac{\int_{A_p} \rho u \, d \, A_p}{\int_{A_p} \rho \, d \, A_p} \tag{9}$$

Finally α_Γ is chosen to match the maximum experimental PO amplitude measured during the second blow. In order to keep the model as simple as possible, a constant parameter is employed for the whole simulated time.

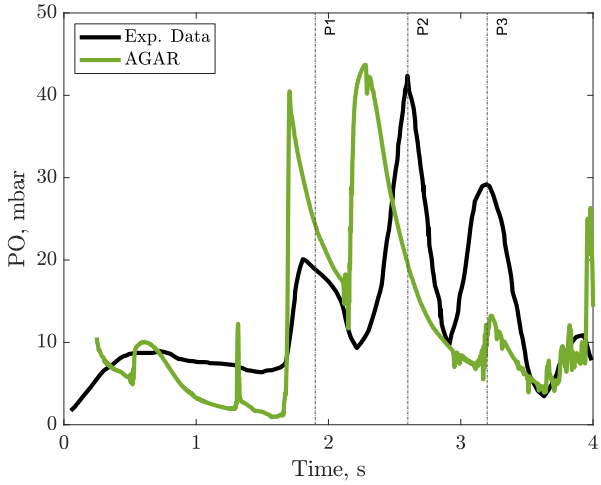

Fig. 5 C1xb pressure oscillations

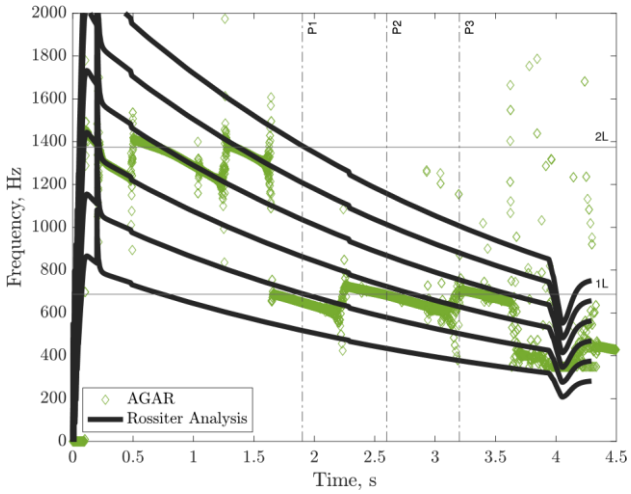

Fig. 6 C1xb frequency patterns

The comparison between numerical and experimental data concerning the pressure oscillations amplitude in time is reported in Fig. 5. A satisfying agreement is obtained in terms of PO time windows: the AGAR solution presents three blows in the second half of the firing time with a lasting very similar to that shown by the experimental data. Major differences are observable for what concerns the PO amplitude since only the second blow peak is well recovered, as was expected given the ad-hoc calibration. Fig. 6 presents the PO frequency evolution over time. In agreement with the experimental data, the first acoustic mode is excited when the three blows actually occur. The typical frequency jumps necessary to shift from one PO blow to another are clearly evident. Focusing on the first phase of the firing, it is possible to see that AGAR is capable of reconstructing the absence of relevant pressure oscillations. Indeed, in this time window, the AGAR frequency pattern is locked on the second mode, actually not able to provide a high-level amplitude instability. This last aspect was for years object of study and, only recently, a massive

numerical simulation has demonstrated the role of laminar-turbulent regime transition in the PO damping (Fabignon *et al.* 2016).

Comparing the Rossiter law with the AGAR frequency results, a very good agreement is notable regarding the decreasing trend and the discrete behavior. On the other hand, it is interesting to observe that the Rossiter semi-empirical approach would predict a coupling on the first mode shortly before one second which is not present in the experimental data and the AGAR solution.

Some discrepancies are still visible in what concerns the instability amplitude and the timing of the second blow. The latter may be influenced by the model calibration, in particular by the k_u coefficient. As shown by the authors in a previous work (Grossi *et al.* 2019), the k_u affects the vortex-shedding frequency and the timing of the appearance of the instability, therefore, a slightly different calibration could deliver an improved agreement. Regarding the PO amplitude scenario, it is worth noting that, for this specific case, it is quite difficult to recover the PO amplitude also using high-fidelity simulations (Vuillot and Casalis 2004), a fact which highlights how the amplitude of the oscillations is influenced by complex physical phenomena not easy to reproduce. Focusing on the first blow, the measured peak shows an amplitude lower than the corresponding numerical one. This could be explained by the fact that the first blow shows up right after the phase characterized by the laminar-turbulent transition, a phenomenon that could still marginally act during the onset of the instability. AGAR does not rely on a specific formulation to model this phenomenon, thus the present amplitude difference should be expected. For what concerns the last blow, the low amplitude of the AGAR solution may be ascribed to a decreased intensity of the vortices which, in turn, is strongly affected by the numerical diffusion when a large number of vortices is present in the domain. Nevertheless, it is important to point out that the ultimate aim of this work is to discuss the possibility to recover the vortex-shedding phenomenon occurring in SRMs, thus a further investigation of the model regarding more specific issues is entrusted to future activities.

An exhaustive scenario regarding AGAR application to C1xb, i.e., the different factors that make up the aeroacoustic feedback loop, is reported in Fig. 7. The second blow at 2.4 seconds is considered since its highest pressure oscillations level. The unsteady velocity field, in Fig. 7(a), shows the typical acoustic first mode, with the two nodes at the extremes (in a SRM with a choked nozzle the motor throat behaves in a similar way to the head wall) and the antinode in the middle of the chamber. The time evolution of the velocity at the propellant grain edge triggers the generation of vortices, shown as peaks of the ω field, which are then convected by the flow towards the nozzle, as shown in Fig. 7(b). During their transport, vortices are affected by numerical diffusion, responsible for the gradual diminishing of the vortices intensity. Finally, the flow itself is further excited by the oscillating behavior of the aeroacoustic sources, presented in Fig. 7(c), which are functions, as stated in Eq. (7) and Eq. (8), of the vorticity field. It is worth noting that these terms are made of the superimposition of a mean quantity and a fluctuating one. This behavior is due to the presence of a minimum value assumed by the vorticity pattern at the end of the chamber which remains constant regardless of the passage of a vortex. This means that a certain amount of the aeroacoustic energy is given to the mean flowfield rather than to the acoustic one. However, this contribution is actually negligible since, as shown by Laureti (2018), the AGAR flowfield is characterized by very few differences, in terms of the ballistic properties, with or without the onset of an aeroacoustic feedback loop.

A further assessment of the AGAR model has been accomplished thanks to a qualitative comparison, presented in Fig. 8, regarding two vorticity fields: one is obtained via the present Q1D

approach, and the other comes from a CFD solution extracted from the work of (Vuillot and Casalis 2004). For the considered time instant, the AGAR solution shows four vortices in the motor chamber, whereas the CFD result presents just three of them. However, this discrepancy is ascribable only to the different origins of vortical structures in the two methods: in AGAR, they are fully generated at the propellant edge, on the contrary, in a CFD computation, they arise only when the shear layer gets unstable enough to roll up, a condition achieved little downstream the geometry discontinuity. It is important to point out that the difference in the number of vortices does not imply a difference in the aeroacoustic loop properties: in the C1xb motor, the emission of the acoustic perturbation is likely to occur in the proximity of the nozzle convergent section, therefore the presence of an extra vortex downstream the propellant edge does not contribute to the aeroacoustic feedback loop. Indeed, what really matters to determine the PO characteristics is the time between two consequent vortices going through the convergent region of the nozzle. Hence, the Q1D and CFD models provide the same conditions regarding vortices velocity and shedding frequency.

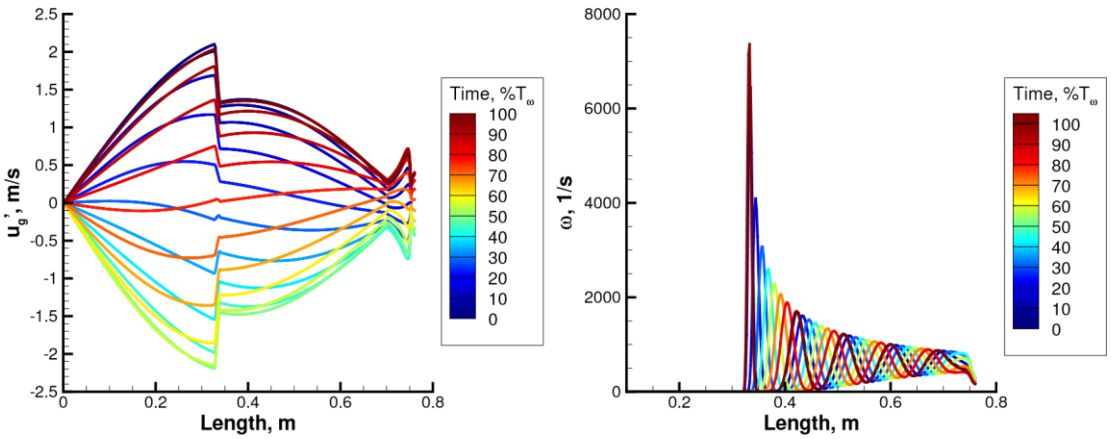

(a) Velocity unsteady field (b) Vorticity field

(c) Aeroacoustic momentum source field

Fig. 7 AGAR aeroacousic feedback loop during one period of oscillation at 2.4 s

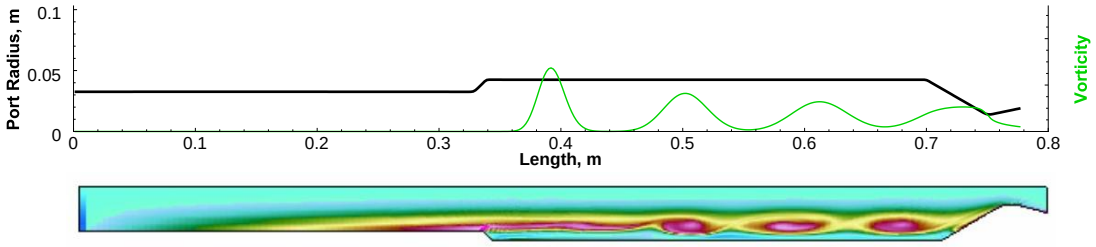

Fig. 8 AGAR vorticity field for C1xb at 2 seconds is compared with a CFD solution (Vuillot and Casalis 2004)

5. Conclusions

The coupling between vortex shedding and pressure oscillations in a small-scale SRM has been investigated through a Q1D model, named AGAR, developed and designed to deal with hydrodynamic instabilities in SRMs. The numerical simulation reproduces the ONERA C1xb during the whole firing time, a motor known to be unstable due to corner vortex-shedding, showing pressure oscillations characterized by the flute-mode behavior. The AGAR calibration setup has been validated via multidimensional analyses for what concerns the vortices velocity and imposed via comparison with the experimental data regarding their intensity. Confronting the PO numerical results with the measured data, a satisfying agreement is found regarding PO time windows of occurrence, while the PO amplitude presents more differences. A comparison with the Rossiter law shows up that the AGAR model accurately follows the computed vortex-shedding frequencies, confirming that the reproduced physical phenomenology is the experimental one. Moreover, contrary to the Rossiter analysis, AGAR recovers the absence of PO during the first firing phase. These results witness how the Q1D methodology may be exploited to build a low-cost tool aimed to deliver a general risk assessment of the motor scenario without recovering all the features present in the physical phenomenology. On the other hand, this purpose may be achieved only after the application of the AGAR model to many different motors so as to make its calibration effectively predictive for future designs.

References

Anthoine, J., Buchlin, J. and Hirschberg, A. (2002), "Effect of nozzle cavity on resonance in large SRM: Theoretical modeling", *J. Propuls. Power*, **18**(2), 304-311. https://doi.org/10.2514/2.5935.

Ballereau, S., Godfroy, F., Gallier, S., Orlandi, O., Thepenier, J., Robert, E. and Cesco, N. (2011), "Evaluation method of thrust oscillations in large SRM-Application to segmented SRMs", *47th AIAA/ASME/SAE/ASEE Joint Propulsion Conference & Exhibit*, 6054.

Bouyges, M., Chedevergne, F., Casalis, G. and Majdalani, J. (2017), "Asymptotically based selfsimilarity solution of the Navier-Stokes equations for a porous tube with a non-circular crosssection", *J. Fluid Mech.*, **826**, 396-420. https://doi.org/10.1017/jfm.2017.430.

Casalis, G., Boyer, G. and Radenac, E. (2011), "Some recent advances in the instabilities occurring in long solid rocket motors", *47th AIAA/ASME/SAE/ASEE Joint Propulsion Conference and Exhibit 2011*.

Cavallini, E. (2009), "Modeling and Numerical Simulation of Solid Rocket Motors Internal Ballistics", Ph.D. Thesis, Department of Aerospace and Mechanical Engineering, Sapienza University of Rome.

Cavallini, E., Favini, B. and Neri, A. (2015), "Q1D modelling of vortex-driven pressure oscillations in Aft-

Finocyl SRMs with submerged nozzle cavity", *AIAA Joint Propulsion Conference*, Orlando, Florida.
Chedevergne, F., Casalis, G. and Feraille, T. (2006), "Biglobal linear stability analysis of the flow induced by wall injection", *Phys. Fluid.*, **18**(1), 014103. https://doi.org/10.1063/1.2160524.
Clements, R.R. (1973), "An inviscid model of two-dimensional vortex shedding", *J. Fluid Mech.*, **57**(2), 321-336. https://doi.org/10.1017/S0022112073001187.
Culick, F. and Kuentzmann, P. (2006), "Unsteady motions in combustion chambers for propulsion systems", Technical Report, NATO Research and Technology Organization Neuilly-Sur-Seine, France.
Culick, F.E.C. (1966), "Acoustic oscillations in solid propellant rocket chambers", *Astronautica Acta*, **12**(2), 113-126.
Dotson, K., Koshigoe, S. and Pace, K. (1997), "Vortex shedding in a large solid rocket motor without inhibitors at the segment interfaces", *J. Propuls. Power*, **13**(2), 197-206. https://doi.org/10.2514/2.5170.
Dotson, K., Womack, J. and Grosserode, P. (2001), "Structural dynamic analysis of solid rocket motor resonant burning", *J. Propuls. Power*, **17**(2), 347-354. https://doi.org/10.2514/2.5748.
Dunlap, R. and Brown, R.S. (1981), "Exploratory experiments on acoustic oscillations driven by periodic vortex shedding", *AIAA J.*, **19**(3), 408-409. https://doi.org/10.2514/3.7783.
Dunlap, R., Blackner, A.M., Waugh, R.C., Brown, R.S. and Willoughby, P.G. (1990), "Internal flow field studies in a simulated cylindrical port rocket chamber", *J. Propuls. Power*, **6**(6), 690-704. https://doi.org/10.2514/3.23274.
Dupays, J., Pr´evost, M., Tarrin, P. and Vuillot, F. (1996), "Effects of particulate phase on vortex shedding driven oscillations in solid rocket motors", *32nd Joint Propulsion Conference and Exhibit*, 3248.
Fabignon, Y., Anthoine, J., Davidenko, D., Devillers, R., Dupays, J., Gueyffier, D., ... & Erades, C. (2016), "Recent advances in research on solid rocket propulsion", *Aerospace Lab*, (11), 15. https://doi.org/10.12762/2016.AL11-13
Fabignon, Y., Dupays, J., Avalon, G., Vuillot, F., Lupoglazoff, N., Casalis, G. and Pr´evost, M. (2003), "Instabilities and pressure oscillations in solid rocket motors", *Aerosp. Sci. Technol.*, **7**(3), 191-200. https://doi.org/10.1016/S1270-9638(02)01194-X.
Ferretti, V. (2011), "Numerical simulations of acoustic resonance of solid rocket motor", Ph.D. Thesis, Department of Aerospace and Mechanical Engineering, Sapienza University of Rome, Italy.
Flandro, G. and Jacobs, H. (1973), "Vortex generated sound in cavities", *Aeroacoustics Conference*, 1014.
Flatau, A. and VanMoorhem, W. (1990), "Prediction of vortex shedding responses in segmented solid rocket motors", *26th Joint Propulsion Conference*, 2073.
Gallier, S. and Godfroy, F. (2009), "Aluminum combustion driven instabilities in solid rocket motors", *J. Propuls. Power*, **25**(2), 509-521. https://doi.org/10.2514/1.37664.
Grossi, M., Bianchi, D. and Favini, B. (2020), "Modeling Multiphase Effects on Pressure Oscillations in Solid Propulsion", *AIAA Propulsion and Energy 2020 Forum*, 3927.
Grossi, M., Laureti, M. and Favini, B. (2019), "Quasi-one dimensional model of pressure oscillations in Aft-Finocyl solid rocket motors: A critical evaluation of alternative closure sub-models and calibrations", *AIAA Propulsion and Energy 2019 Forum*, 4137.
Hijlkema, J., Pr´evost, M. and Casalis, G. (2011), "On the importance of reduced scale Ariane 5 P230 solid rocket motor models in the comprehension and prevention of thrust oscillations", *CEAS Space J.*, **1**(1-4), 99-107. https://doi.org/10.1007/s12567-011-0008-8.
Hirschberg, L., Hulshoff, S.J., Collinet, J., Schram, C. and Schuller, T. (2018), "Vortex nozzle interaction in solid rocket motors: A scaling law for upstream acoustic response", *J. Acoust. Soc. Am.*, **144**(1), EL46-EL51. https://doi.org/10.1121/1.5046441.
Howe, M. (1998), *Acoustics of Fluid-Structure Interactions*, Cambridge University Press, New York.
Larrieu, S., Godfroy, F., Orlandi, O., Robert, E., Ciucci, A. and Cesco, N. (2015), "Demonstration of pressure oscillation reduction in the frame of new launchers development", *6th European Conference for AeroSpace Sciences*, Krakov, Poland.
Larrieu, S., Orlandi, O., Godfroy, F. and Di Trapani, C. (2018), "Two minutes inside P120C SRM", *Space Propulsion 2018*, Seville, Spain.
Laureti, M. (2018), "Pressure oscillations in Aft-Finocyl SRMs", Ph.D. Thesis, Sapienza University of

Rome, Italy.
Laureti, M. and Favini, B. (2019), "Pressure oscillations in aft-finocys SRMs", *AIAA SciTech Forum*, San Diego, California, USA.
Laureti, M., Favini, B., Rossi, G. and Paglia, F. (2018), "P80 SRM pressure oscillations reconstruction", *2018 Joint Propulsion Conference*, 1-11.
Lupoglazoff, N. and Vuillot, F. (1996), "Parietal vortex shedding as a cause of instability for long solid propellant motors. Numerical simulations and comparisons with firing tests", AIAA Paper.
Majdalani, J., Ramesh Kumar, T. and Akiki, M. (2021), "On the compressible biglobal stability of the mean flow motion in porous tubes", *Phys. Fluid.*, **33**(8), 083109. https://doi.org/10.1063/5.0057886.
Mastrangelo, G., Morillon, T., Scoccimarro, D., Lambiase, E., Guenot, L., Paradis, L., Planquart, P., Supi´e, P., Cesco, N., Breteau, J., Leblin, J.P. and Revel, D. (2013), "POD-X program: Towards the SRM pressure oscillation demonstrator first firing test", *49th AIAA/ASME/SAE/ASEE Joint Propulsion Conference*, Volume 1 PartF.
Matveev, K. and Culick, F. (2003), "A model for combustion instability involving vortex shedding", *Combus. Sci. Technol.*, **175**(6), 1059-1083. https://doi.org/10.1080/00102200302349.
Orlandi, O., Plaud, M., Godfroy, F., Larrieu, S. and Cesco, N. (2019), "Aluminium droplets combustion and SRM instabilities", *Acta Astronautica*, **158**, 470-479. https://doi.org/10.1016/j.actaastro.2019.03.036.
Rossiter, J. (1964), "Wind-tunnel experiments on the flow over rectangular cavities at subsonic and transonic speeds", Aeronautical Research Council Reports & Memoranda.
Taylor, G.I. (1956), "Fluid flow in regions bounded by porous surfaces", *Proc. Roy. Soc. London. Ser. A. Math. Phys. Sci.*, **234**(1199), 456-475. https://doi.org/10.1098/rspa.1956.0050.
Telara, M., Paglia, F., Stella, F. and Giangi, M. (2006), "ARIANE 5 P230 SRM Frontal Thermal Protection evolution: Numerical simulation", *42nd AIAA/ASME/SAE/ASEE Joint Propulsion Conference & Exhibit*, 5242.
Vuillot, F. and Casalis, G. (2004), "Motor flow instabilities-Part 1", Technical Report, Internal Aerodynamics in Solid Rocket Propulsion RTO-EN-023, NATO-RTO.
Yang, H.Q., West, J. and Harris, R.E. (2018), "Coupled fluid-structure interaction analysis of solid rocket motor with flexible inhibitors", *J. Spacecraft Rocket.*, **55**(2), 303-314. https://doi.org/10.2514/1.A33947.